SANDIA REPORT

SAND2016-9678
Unlimited Release
Printed August, 2016

Detector Response Function and Directional Gamma-Ray Source Calculations for Polaris

Dean J. Mitchell, Steven M. Horne, Gregory G. Thoreson, Lee T. Harding, and Sean O'Brien

Prepared by
Sandia National Laboratories
Albuquerque, New Mexico 87185 and Livermore, California 94550

Sandia National Laboratories is a multi-program laboratory managed and operated by Sandia Corporation, a wholly owned subsidiary of Lockheed Martin Corporation, for the U.S. Department of Energy's National Nuclear Security Administration under contract DE-AC04-94AL85000.

Issued by Sandia National Laboratories, operated for the United States Department of Energy by Sandia Corporation.

Available to DOE and DOE contractors from
U.S. Department of Energy
Office of Scientific and Technical Information
P.O. Box 62
Oak Ridge, TN 37831

Telephone: (865) 576-8401
Facsimile: (865) 576-5728
E-Mail: **reports@osti.gov**
Online ordering: **http://www.osti.gov/scitech**

Available to the public from
U.S. Department of Commerce
National Technical Information Service
5301 Shawnee Rd
Alexandria, VA 22312

Telephone: (800) 553-6847
Facsimile: (703) 605-6900
E-Mail: **orders@ntis.gov**
Online order: **http://www.ntis.gov/search**

SAND2016-9678
Unlimited Release
Printed August, 2016

Detector Response Function and Directional Gamma-Ray Source Calculations for Polaris

D.J. Mitchell, S.M. Horne, G.G. Thoreson, L.T. Harding, and Sean O'Brien
Nuclear Threat Science, 6634
Sandia National Laboratories
P.O. Box 5800
Albuquerque, New Mexico 87185-MS0782

Abstract

A Directional Unfolded Source Term (DUST) method was developed to compute directionally resolved gamma-ray source terms based on back-projection spectra synthesized by Compton Cameras. Spectral features in the unprocessed spectra are indistinct primarily because the rotational angles for the conical projections cannot be determined, so probability distributions are constructed from overlapping cones. The DUST method uses an angular response function to compute a covariance matrix, which is used to process count rates in back-projection spectra by linear regression to partition the gamma-rays among several spatial regions. This method was applied to analyze data collected by the Polaris detector during an evaluation that was conducted at Oak Ridge National Laboratory (ORNL). The evaluation includes measurements of calibration sources with angular separations ranging from 1° to more than 50°. Measurements were also performed for cylindrical depleted uranium castings and a ^{137}Cs source inside a large polyethylene sphere.

The DUST algorithm was able to differentiate gamma-rays emitted by ^{137}Cs and ^{60}Co when the sources were separated by less than 2°, but separation greater than 10° was required to isolate the ^{133}Ba emission from gamma-rays emitted by the other sources. The computed source terms were consistent with emission profiles from the calibration sources and from models of the spatially-extended sources. Methods for viewing radiation profiles were also evaluated because user input is required to select spatial regions of interest.

ACKNOWLEDGEMENTS

This work was funded by DOE/NNSA/NA-221 under project number SL15-V-DirectSoftware-PD2Jc.

CONTENTS

FIGURES

TABLES

NOMENCLATURE

API	Application Programming Interface
Ba	Barium
CA	Coded Aperture
CC	Compton Camera
Co	Cobalt
Cs	Cesium (Cesium)
CZT	Cadmium Zinc Telluride
DLL	Dynamic Link Library
DRF	Detector Response Function
DU	Depleted Uranium
DUST	Directional Unfolded Source Term
EIID	Energy-Imaging Integrated Deconvolution
FWHM	Full-width-at-half-maximum
GADRAS	Gamma Detector Response and Analysis Software
GeGI	Germanium Gamma Imager
ORNL	Oak Ridge National Laboratory
PE	Polyethylene
RGB	Red, Green, and Blue
SNL	Sandia National Laboratories

1 INTRODUCTION

Gamma-ray detectors have been developed that synthesize images of radiation sources based on Compton Camera (CC) and Coded Aperture (CA) methods. In the CC approach, a Compton scatter event followed by an absorption of the scattered gamma-ray yields a conical probability distribution for the inferred scatter angle. Images are constructed by summing the probability distributions for numerous overlapping interactions. The CA method is an alternative imaging approach that places a mask between the source and a pixelated detector to create shadow patterns, which are processed to construct gamma-ray images. Since the CC method only tallies events corresponding to at least two interactions within the detector, it is most effective for high-energy gamma rays. In contrast, the CA method is more suitable for low-energy gamma rays, which are stopped by masks composed of high-atomic-number materials. Some imaging sensors apply both methods to extend the operational gamma-ray energy range.

All CC imagers and most CA sensors utilize spectroscopic detectors, and gamma-ray energies are determined for each interaction. Although directional sensors can also function as spectroscopic detectors, most development has focused on optimization of gamma-ray images. The objective of this paper is to document work performed at Sandia National Laboratories (SNL) as part of the DirectSoftware project, [1] which seeks to develop the ability to efficiently process and analyze spectroscopic data collected by gamma-ray detectors with directional capabilities. Potential advantages are the ability to distinguish features of spatially separated radionuclides and to identify weak sources in the presence of larger radiation backgrounds. The overall DirectSoftware project has a broad scope, but this document focuses on the utilization of Compton back-projection spectra collected by the Polaris system, which is a Cadmium Zinc Telluride (CZT)-based directional spectrometer manufactured by H3D Inc.

This work leverages components of the Gamma Detector Response and Analysis Software (GADRAS), which incorporates Detector Response Function (DRF), radiation transport, and radiation analysis capabilities [2] [3] [4]. Adding the ability to process data collected by directional spectrometers as an integral function of GADRAS will enable the efficient application of analysis tools that is already familiar to many spectroscopists. Data collected by Polaris and the Germanium Gamma Imager (GeGI) is accessed by an Application Programming Interface (API) and Dynamic Link Libraries (DLLs), which were developed jointly by H3D, Oak Ridge National Laboratory (ORNL), the University of Michigan, and SNL.

This page in intentionally blank.

2 POLARIS DETECTOR

The Polaris detector incorporates 18, 2 cm×2 cm×1.5 cm CZT detectors that are stacked in two planes. Figure 1 shows the arrangement of crystals in V2.0 and V2.1 Polaris systems. The use of pixelated CZT crystals and analog electronics provides a discrete pixel position resolution of 1.7 mm and a depth position resolution of <0.5 mm. Software provided with the Polaris system automatically generates sum spectra, which includes all detection events regardless of the number of interactions. Energies are summed and treated as a single detection if multiple pixels record simultaneous energy depositions. List mode files can be post-processed to generate back-projection spectra. Back-projection spectra apply probability distributions to synthesize spectra for specified ranges of scatter angles. Back-projection spectra referenced in this document were generated using scripts processed by GADRAS, which calls the DLL provided by H3D to synthesize the spectra for a variety of test conditions. The back-projection spectra are represented as counts per channel for the specified angular groups. The processing software provided by H3D also returns uncertainties for the count rates.

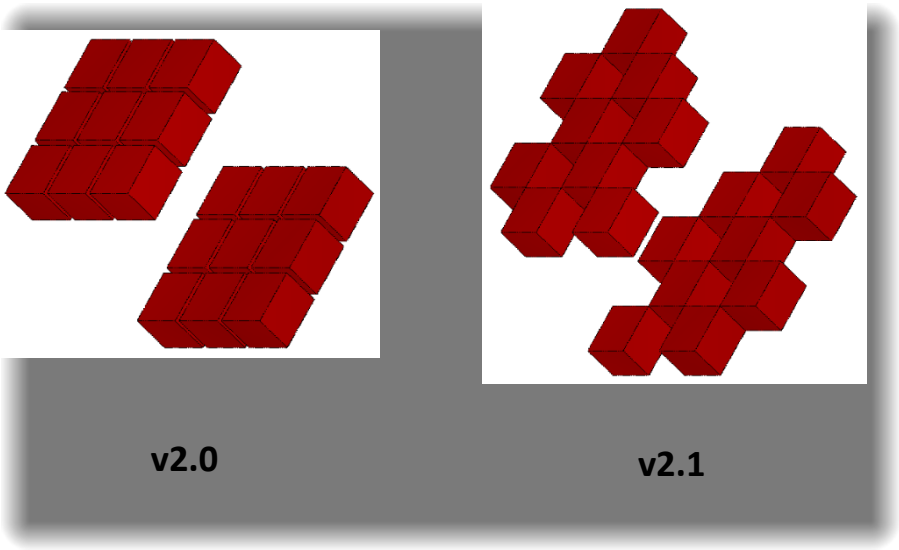

Figure 1. Configuration of CZT Crystals in Polaris Versions V2.0 and V2.1.

This page in intentionally blank.

3 EXPERIMENTAL PROCEDURE

A series of measurements were performed at ORNL using a Polaris V2.1 sensor.[1] The sensor was placed on a table 100 cm from a low-mass stand to which calibration sources were attached. The sources were positioned in a planar grid arrangement where each source was displaced by the same amount in the vertical and horizontal directions relative to the central point. Table 1 lists the displacements and the corresponding angular separations between the closest sources. Figure 2 shows an optical image recorded by Polaris with sources displaced by 20 cm in vertical and horizontal directions relative to the center of the array. The overlay in the upper-left quadrant represents the emission profile for ^{133}Ba as determined by the H3D processing software. The GeGI detector is located at the center of the field of view, on the far side of the calibration source array. Table 2 lists activities of the calibration sources at the time the measurements were performed. Measurement durations were approximately one hour except where noted otherwise.

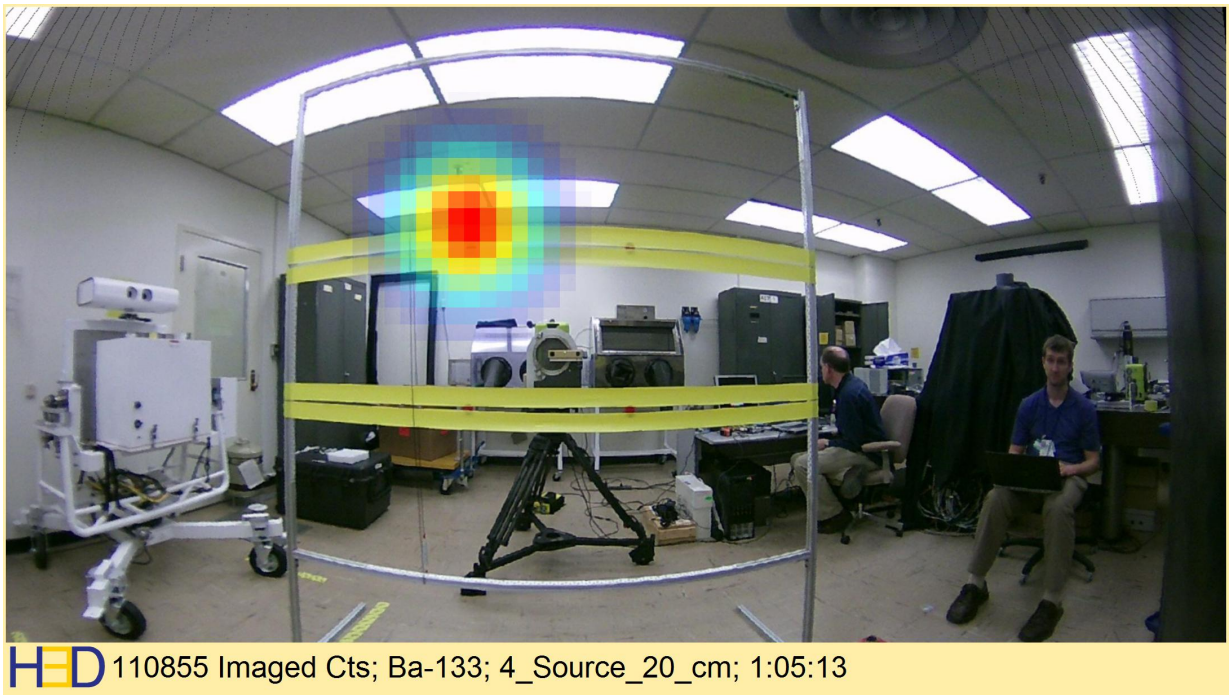

Figure 2. An gamma-ray image of the 133Ba source is superimposed over a photograph taken by the optical camera in Polaris while calibration sources were separated by ±20 cm in vertical and horizontal directions. The GeGI detector is opposite Polaris on the far side of the calibration sources (center of the field of view).

[1] Measurements were also performed using a GeGI detector and coded aperture reconstruction software that was developed at ORNL, but these results are not reported in this document.

Table 1. Source Displacements and Angular Separations

Source Displacements (cm) in Vertical and Horizontal Directions Relative to the Center	Angular Separation Between Closest Sources (degrees)
1	1.1
2	2.3
5	5.7
10	11.4
15	17.1
20	22.6
30	33.4
50	53.1

Table 2. Calibration Sources Used During the ORNL Measurements

Radionuclide	Activity (μCi)
^{241}Am	106.3
^{133}Ba	65.5
^{137}Cs	82.9
^{60}Co	38.3

4 DETECTOR RESPONSE FUNCTION

4.1 Sum Spectra

GADRAS applies an analytic response function to compute photopeak probabilities, radiation continua resulting from gamma rays that scatter out of detectors, and other features such as escape peaks. Continua associated with radiation that scatters into detectors are computed by interpolating a pre-computed library[2] of environmental scatter calculations and application of an empirical model for local scattering. GADRAS applies a scalar to adjust the spectra for multi-element sensors that sum individual elements. Polaris spectra differ from simple sum spectra because energies of simultaneous interactions are summed as a single detection event, which slightly improves the photopeak efficiency, but the difference is small compared to simple sum spectra. Empirical adjustments are applied to refine the accuracy of computed spectra as needed. Figure 3 compares computed spectra with measured sum spectra recorded by a Polaris V2.1 unit at ORNL.

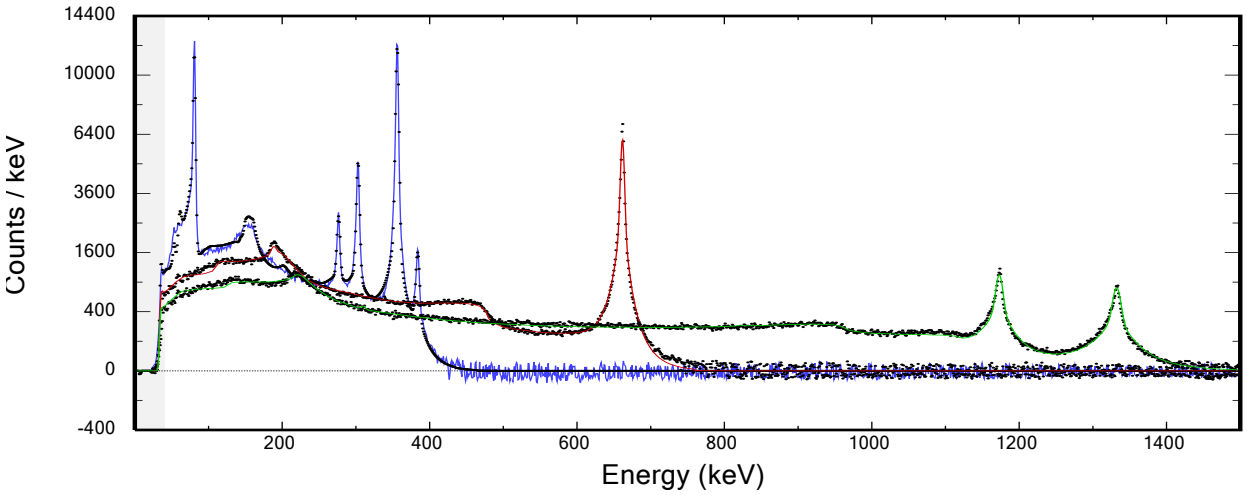

Figure 3. Measured sum spectra (black dots) for ^{133}Ba (blue), ^{137}Cs (red) and ^{60}Co (green) are compared with calculations.

Measurements of ^{133}Ba, ^{137}Cs and ^{60}Co are compared with computed sum spectra, which are represented by blue, red, and green curves, respectively. All of the measured spectra are represented by black dots.

4.2 Back-projection Spectra

The subroutine that GADRAS uses to compute the Compton continuum for single element detectors was modified to compute back-projection spectra. At least two interactions are required to derive the angle from which a gamma-ray originated. Photoelectric absorption of the incident gamma-ray or interactions where the initial recoil photon escapes the array are not tallied. Events

[2] MCNP was used to compute the scatter library.

for which the scattered photon is absorbed on the second or third interaction are scored in the accrued photopeak probability. Incomplete absorption of the scattered photon following two or more interactions are accrued in continuum regions of the spectra. Hence, continua in the back-projection spectra represent incorrectly scored events as well as scattered radiation and Bremsstrahlung radiation from sources such as depleted uranium. The detector response calculations are performed using an analytic model, and probabilities are assigned to each type of interaction.

The normal parameter set that GADRAS applies for detector characterization contains the dimensions of the detector and a representation of the energy resolution and peak shape. The chemical composition of the detector material defines cross sections for photoelectric absorption, Compton scatter, pair production, and x-ray escape. Three additional parameters, defined below, were added to describe the CC response:

- *Spatial Coverage* is the percent of space that is intercepted by other detector elements.
- *Correct Pixel* is the percent of events that are scored in the correct spatial element.
- *Angular Resolution* is the angular resolution in degrees that is applied when back-projection spectra are computed. Although the actual resolution varies with gamma-ray energy, we do not model this effect. The precise value of resolution is obscured by correlations with other parameters in the DRF model, so the angular resolution parameter is fixed at 10° for both V2.0 and V2.1 Polaris units.

Detector characterization enables accurate computation of spectra over the gamma-ray energy range of interest. The response function must also replicate variations of the spectra as a function of the acceptance angle of back-projection spectra. Researchers at the University of Michigan have developed an Energy-Imaging Integrated Deconvolution (EIID) method [5] that tracks all of the interactions, but the exact computation for an array of pixelated CZT crystals is extremely complex and computationally demanding. The approach pursued with GADRAS computes an approximate solution using an analytic detector response model, and then applies empirical adjustments as needed. This approach is not as convenient as the characterization process for non-imaging detectors because the empirical parameters must be adjusted for each detector configuration,[3] but the accuracy is sufficiently good to enable the exploratory effort described in this document. The accuracy is illustrated in Figure 4, which compares measured and computed back-projection spectra for a ^{60}Co source for three ranges of acceptance angles.

[3] Different empirical adjustments are applied for Polaris V2.0 and V2.1.

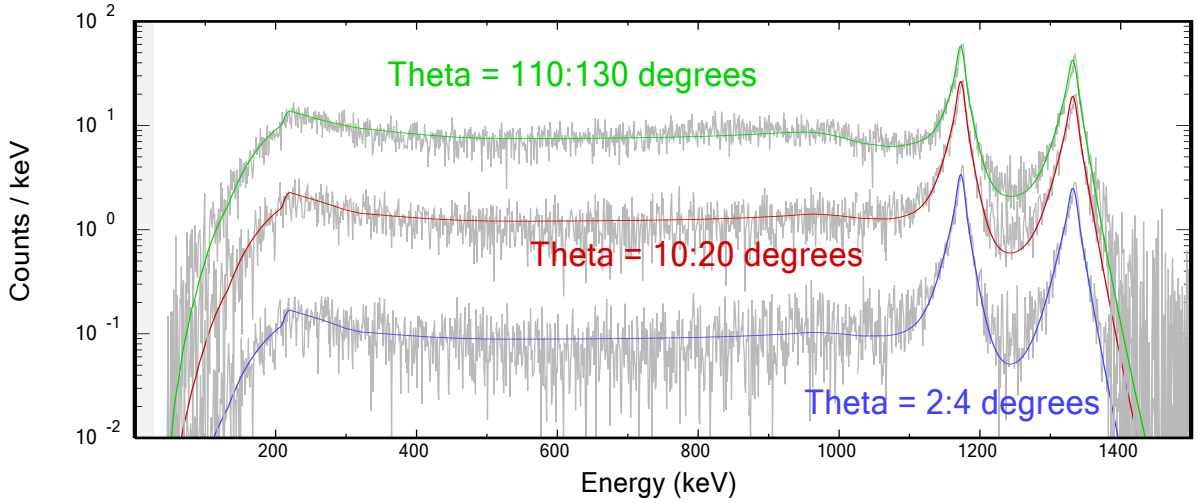

Figure 4. Back-projection spectra measured by Polaris V2.1 (gray) are compared with calculations for three angular groups.

Back-projection spectra measured by Polaris when exposed to a ^{60}Co source are compared with spectra that are computed by GADRAS for three ranges of acceptance angles. The gray traces represent the measured spectra.

Spectra that are displayed in Figure 4 correspond to three ranges of acceptance angles relative to the reference position of the source. The source was located normal to the plane of CZT crystals on the side of the coded aperture mask,[4] which corresponds to θ=0° with respect to the reference position θ_r=90°, φ_r=90°. The full-energy peaks are apparent for all acceptance angles because conical projections include all spatial regions that are consistent with the computed scatter angle. Differences in magnitudes for these spectra derive primarily from variations in the solid angle associated with the angular acceptance angles.[5] Differences in shapes of back-projection spectra are more clearly illustrated by dividing the count rates by the solid angle. Figure 5 compares measured back-projection spectra for the ^{137}Cs source after scaling by the solid angle. With the exception of a small angular range relative to the true source position, the magnitudes of the continua are relatively insensitive to the acceptance angle. Although the peak intensities are greatest in the source direction, differences in intensities are relatively subtle.

[4] Although we do not discuss processing data in coded aperture mode in this paper, a tungsten coded aperture mask was present when the measurements were performed.

[5] This is addressed by the *Correct Pixel* parameter in the detector response function.

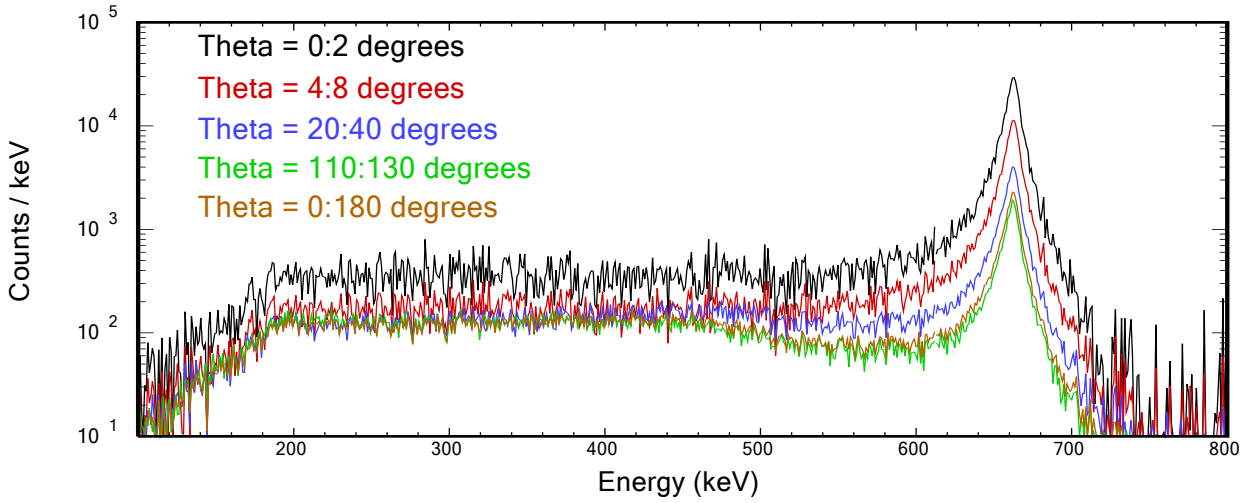

Figure 5. Measured back-projection spectra for ^{137}Cs in several angular groups are compared after dividing the count rates by the solid angles associated with the acceptance angles.

5 THEORY

5.1 Directional Gamma-Ray Source Terms

Compton back-projection spectra exhibit features that vary with the acceptance angle, relative to the actual source location; so it should be possible to derive gamma-ray spectra as a function of position. However, achieving this goal is challenging because there are strong covariances among the source terms and back-projection spectra. Furthermore, differences in the directional response may be smaller than statistical and computational uncertainties. The goal of this effort is to document what approaches worked versus those that were less successful.

The Directional Unfolded Source Term (DUST) approach that we developed uses the DRF to determine source terms for multiple spatial regions based on a series of back-projection spectra. The method proceeds as follows:

- Starting at the highest energy group, solve for source terms in each spatial group, where $S_{i,k}$ is the source term in energy group i and spatial group k. This is achieved by applying linear regression to solve for $S_{i,k}$ in the following equation:

$$Y_{i,j} = \sum_{k=1}^{nAngles} R_{i,\theta_{j,k}} S_{i,k} \tag{1}$$

  where $Y_{i,j}$ is the number of counts in energy group i and spatial group j, and $R_{i,\theta_{j,k}}$ is the full energy response for energy group i at an angle $\theta_{j,k}$ between spatial groups j and k. Since the spatial groups have finite extent, values of $R_{i,\theta_{j,k}}$ are determined by averaging over the extents of the spatial groups j and k. The response matrix, $\boldsymbol{R}$, was determined by characterizing the response for back-projection spectra as described in Section 4.2. The resolution was set to zero when computing $\boldsymbol{R}$ in order to avoid imposing additional broadening, relative to the intrinsic resolution of the detector.

- After solving for $S_{i,k}$, the continuum response can be stripped from the back-projection spectra as follows:

$$Y_{1:i-1,j} = Y_{1:i-1,j} - \sum_{k=1}^{nAngles} R_{1:i-1,\theta_{j,k}} S_{i,k} \tag{2}$$

- The value of i is decremented and the process is repeated until i=1.

The DUST process produces gamma-ray profiles for each of the spatial groups that are represented in the set of back-projection spectra represented in the input file. Stripping the continua, as the spectra are processed according to Eq. (2), eliminates the continuum component of the DRF. Thus, $S_{i,k}$ should represent discrete gamma rays as well as radiation continua emanating from radiation sources. However, stripping the continua according to Eq. (2) did not work well in practice because statistical and computational errors tended to lead to unstable

solutions, where the source profiles exhibited sequences of channels with low emission rates followed by channels with high emission rates, and the instability increased as the errors propagated to lower energy. Better results were obtained by solving for the entire source matrix, ***S***, without applying Eq. (2), then stripping the continuum according to Eq. (3).

$$S_{1:i-1,j} = S_{1:i-1,j} - \sum_{k=1}^{nAngles} R'_{1:i-1,\theta_{j,k}} S_{i,k} \tag{3}$$

The response matrix R' that is applied using Eq. (3) was determined by fitting the residuals after applying the DUST method for individual calibration sources. The DRF matrices ***R*** and R' are not identical, but they have similar significance.

In principal, the application of linear regression to solve Eq. (1) is straightforward, but the source terms do not always represent credible solutions. For example, the combination of a negative source term plus a positive source term can cancel out such that the net response is near zero. Since a negative gamma-ray leakage is not possible, the negative term could either be eliminated or constrained. The best performance was obtained by adding constraints such that the number of observables that are fit by linear regression exceeds the number of variables (i.e., $S_{i,k}$ in Eq. 1). The constraints are applied for any term where $S_{i,k}$ is negative. The value of $S_{i,k}$ is constrained to the previous solution, $S_{i+1,k}$, if the energy group falls within one full-width-at-half-maximum (FWHM) of a spectral peak centroid, or the constraint is set to zero outside of peak regions. Initial variances for the constraints are large (i.e., weak constraints). The variance estimates are reduced by a factor of ten and the regression fit is repeated for up to six iterations while negative source terms are returned. One advantage of applying this approach as opposed to setting $S_{i,k}$ to zero and eliminating the term from the regression fit is that the application of selective constraints imposes smaller biases on the estimated uncertainties. Source terms that initially have negative values may also yield positive (i.e., feasible) values after other terms are constrained.

6 RESULTS AND DISCUSSION

6.1 Graphic Display of Data Collected by Directional Sensors

The GADRAS application was augmented to display back-projection spectra intensity profiles derived from recorded list-mode data. The interface enables the display of either gross intensity profiles or energy resolved profiles, where different colors are coded to represent specified energy regions. The latter approach is illustrated in Figure 6, where red, green, and blue (RGB) represent the peak regions for ^{133}Ba, ^{137}Cs, and ^{60}Co, respectively. This screen capture corresponds to the measurement configuration where sources are displaced by ±50 cm in vertical and horizontal directions relative to the central point. The ^{133}Ba source is located in the upper-left quadrant, ^{60}Co is in the lower-left quadrant, and ^{137}Cs is in the lower right position. An ^{241}Am source was placed in the upper-right quadrant, but the low-energy gamma rays emitted by ^{241}Am are not observed in Compton back-projection spectra because of the low scatter probability and lower-level discriminator settings. It is notable that the red region is broader than the blue region because the angular resolution is worse for low-energy gamma rays.

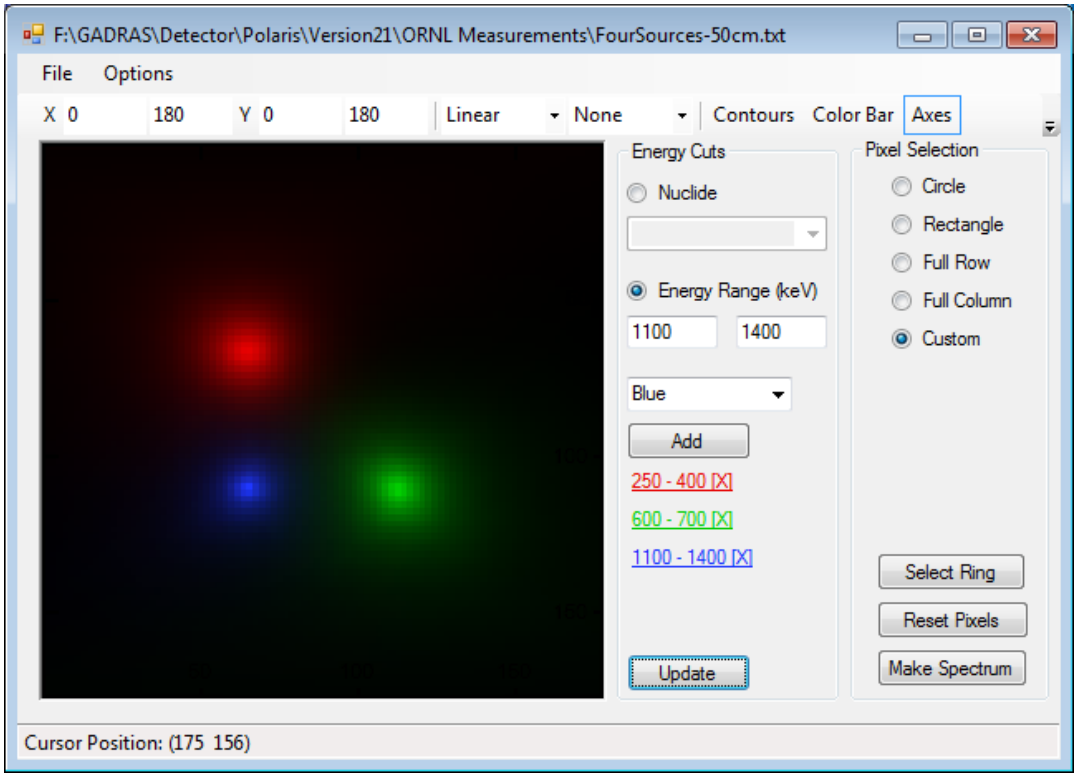

Figure 6. The energy-resolved intensity profile displayed in this plot corresponds to the configuration where the calibration sources are displaced by 50 cm relative to the central point. The horizontal axis corresponds to displacement in the θ direction (horizontal rotation) and the vertical axis is the φ direction (vertical rotation) relative to the reference position θ_r=90°, φ_r=90°.

Figure 7 presents the energy-resolved intensity profile for the configuration where the sources were displaced by 10 cm relative to the central point. Differences in intensities for the three energy regions are visible, but much less resolved. The RGB values representative colors additively, so an equal amount of each color creates a white region, as illustrated in Figure 8, which shows the profile for the calibration sources at 1 cm displacements relative to the center. The upper-left quadrant is slightly red, and the lower-right quadrant is slightly green, so some energy profile information is conveyed even when the sources are nearly collocated.

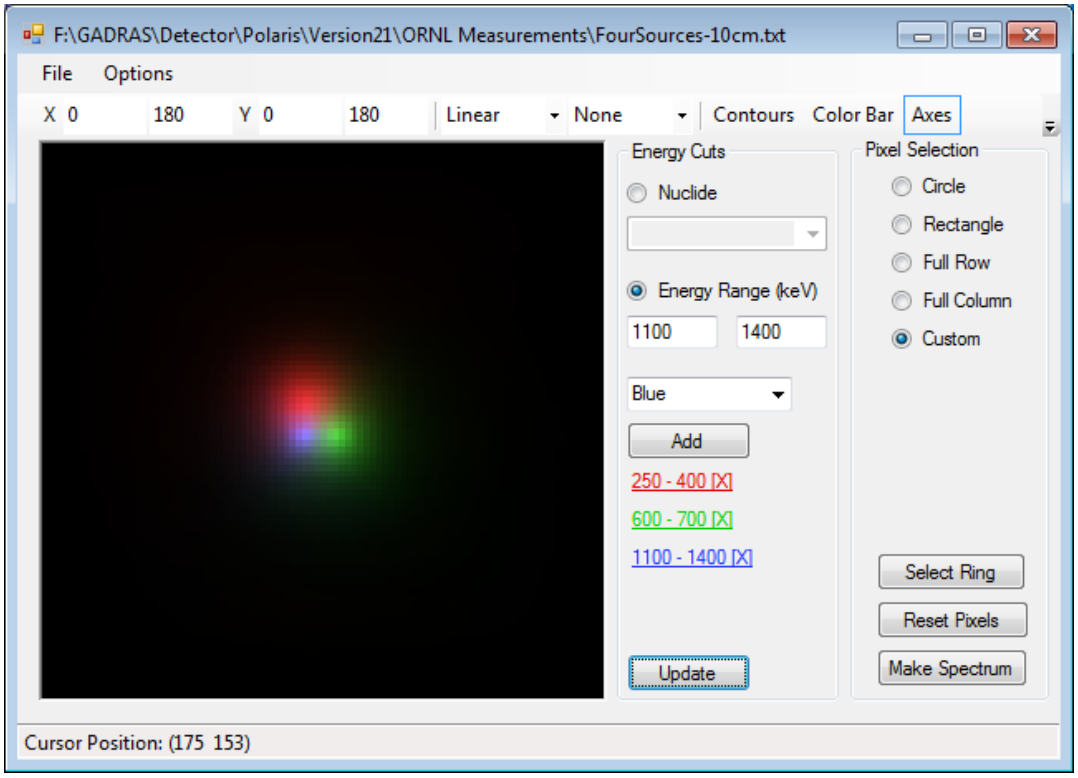

Figure 7. The energy-resolved intensity profile displayed in this plot corresponds to the measurement where sources were displaced by 10 cm relative to the central point.

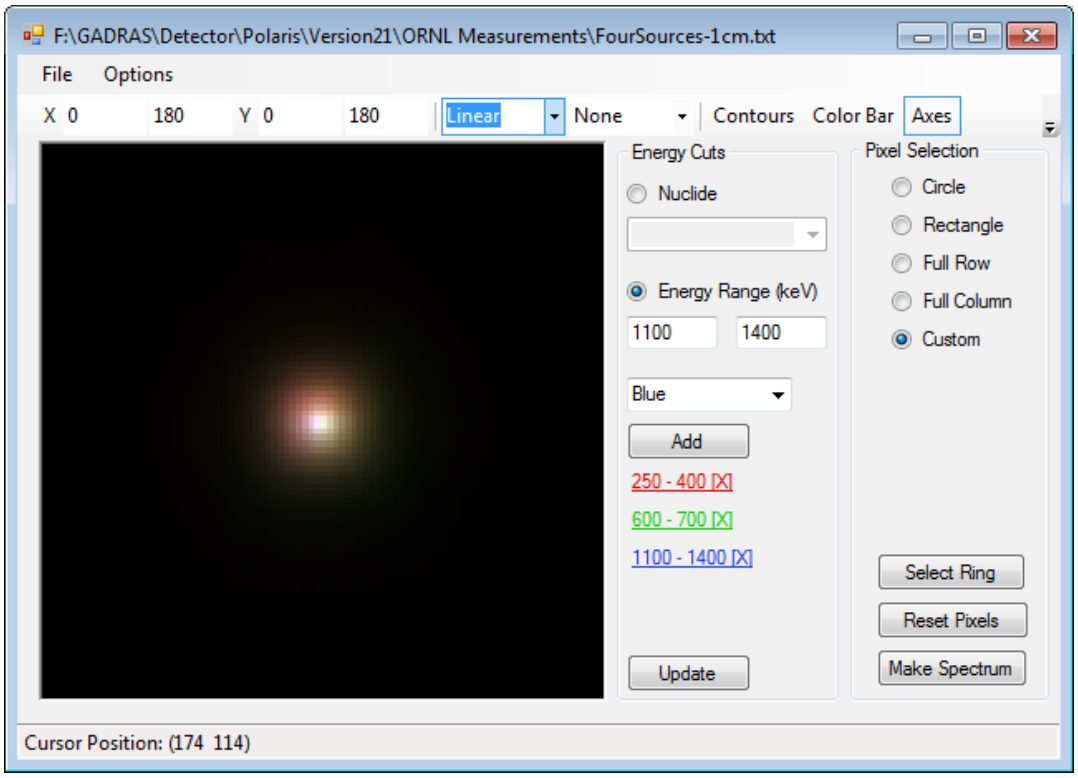

Figure 8. This energy-resolved intensity profile corresponds to the measurement where sources were displaced by 1 cm relative to the central point.

6.2 Spatially Resolved Gamma-Ray Source Terms

6.2.1 Source Terms for Bare Calibration Sources

Spatially resolved radiation source terms were computed for each source configuration using the DUST method. As discussed in Section 5.1, the best results were obtained by using Eq. (3) to strip the continuum after having completed computation of the source matrix $\boldsymbol{S}$. The results are presented in this section.

Several angular groupings were explored to optimize the performance of the DUST algorithm. The best results were obtained using spatial groups within 10° ranges of the actual source positions plus a background group that encompassed all imageable data (i.e., all events resulting in at least two interactions within the detector). Results obtained for 5° ranges were substantially worse, which we attribute primarily to larger statistical uncertainties associated with small solid angles. Acceptance angles substantially greater than 10° degraded the ability to separate emissions from closely spaced sources. Although the results could be improved slightly in some cases by using bulls-eye projections around the sources, the differences were not sufficiently compelling to warrant the additional complexity imposed on data preparation and execution.

Figure 9 shows back-projection spectra used as input to the DUST method for the 10-cm source separation case. The spectra are scaled by the solid angles and rendered with a reduced number of energy groups to facilitate the comparison of spectral shapes for these groups. Labels that are presented on the graph correspond to our convention of representing the range of θ and φ with respect to the actual source position, which is specified as Ref=θ_r,φ_r. The background spectrum accepts all of space, so the reference position is ignored for the background group. Although differences in spectral shapes for the 10°-wide groups are small, the peak intensities are greatest for gamma rays emitted by sources in the specified quadrants. Differences among the spectral shapes are even smaller at closer source spacing.

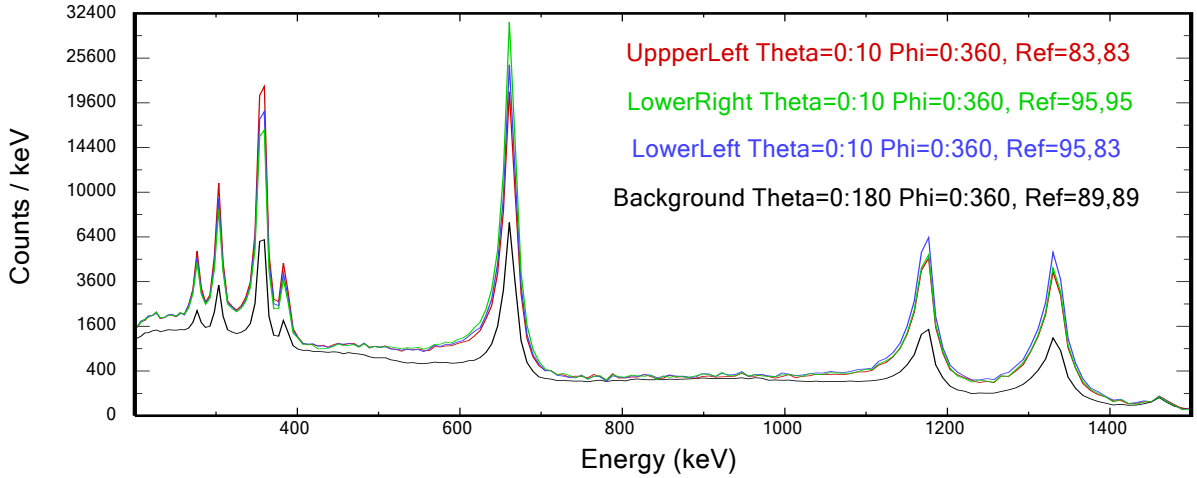

Figure 9. Back-projection spectra for the configuration where sources are displaced ±10 cm from the center are displayed for three 10°-wide angular groups (red, green, and blue) and the background group (black).

Results that are presented in this section should be placed into the context of our objectives, which are listed below.

- Resolve gamma-ray emissions for closely-spaced radiation sources.
- Derive accurate source terms and uncertainty estimates.
- Complete the processing quickly so that the process is suitable for real-time applications. Although computation of the source terms is completed within a few seconds once the back-projection spectra are synthesized, preparation of the back-projection spectra using the H3D DLL can take a few minutes for large list mode files. However, preparation of back-projection spectra could be accelerated or even performed while data are collected if the process is performed systematically and spatial groupings are predetermined.

Figures 10 through 17 present graphic representations of the source terms for all of the source configurations. The background spectra estimated by the DUST method are stripped from the local source terms, so these plots represent excess emission originating within 10°-wide

projections in the directions where the sources are located. As shown in Figure 10, emissions from ^{137}Cs and ^{60}Co are largely associated with the proper quadrants even at displacements of 1 cm relative to the center of the source array, corresponding to 1.1° between the closest sources. This was a surprising finding because there is substantial overlap between the spatial regions with 10°-wide acceptance angles. At this separation distance, the gamma rays emitted by ^{133}Ba are attributed approximately equally to the upper-left (where the source was actually located) and the lower-right quadrant (corresponding to the ^{137}Cs source). The ^{137}Cs and ^{60}Co are well separated at 2-cm displacements, but ^{133}Ba is not resolved until the displacements are 10 cm (11° between closest sources) or more.

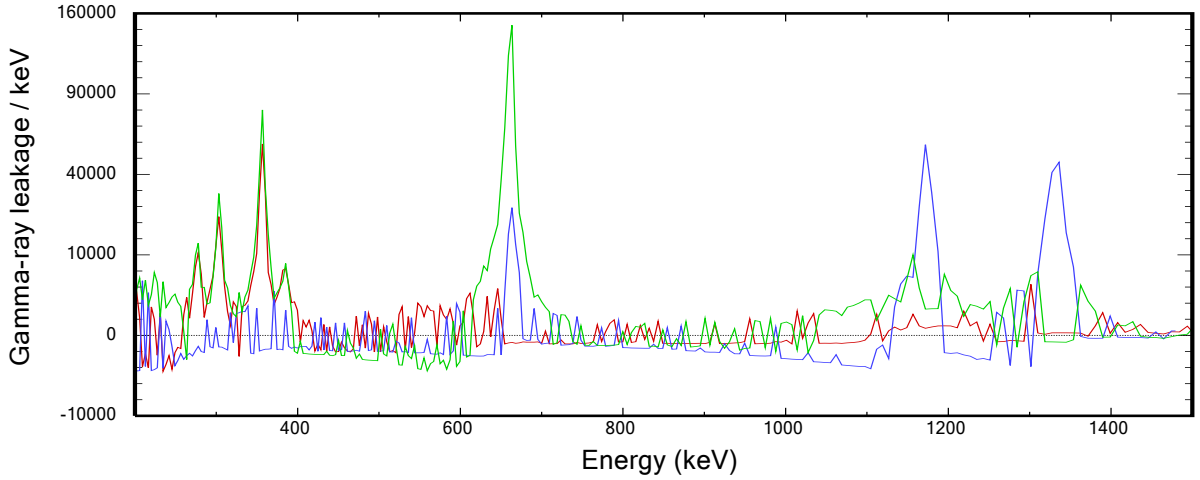

Figure 10. Angular source terms for calibration source displaced 1 cm from center.

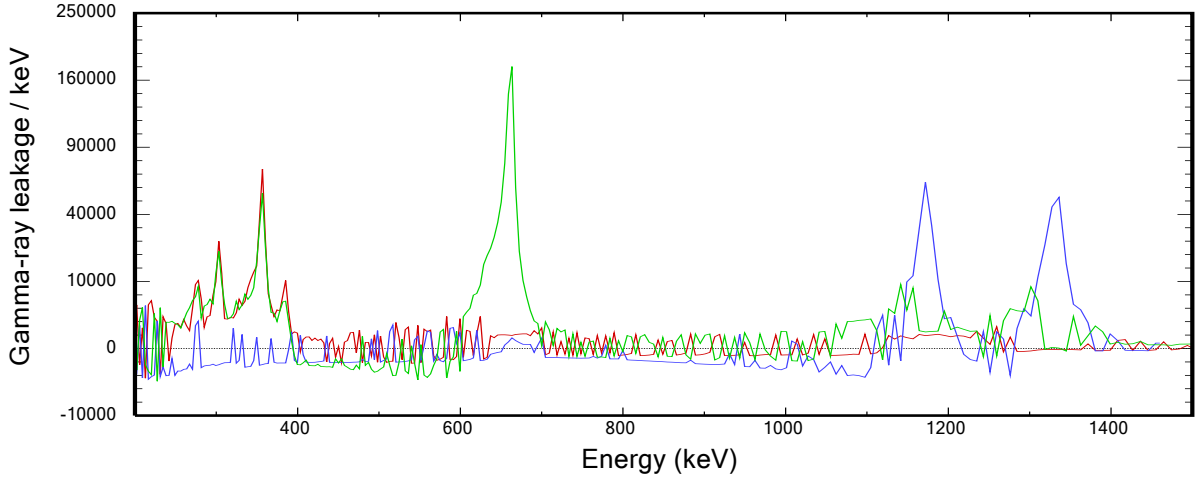

Figure 11. Angular source terms for calibration source displaced 2 cm from center.

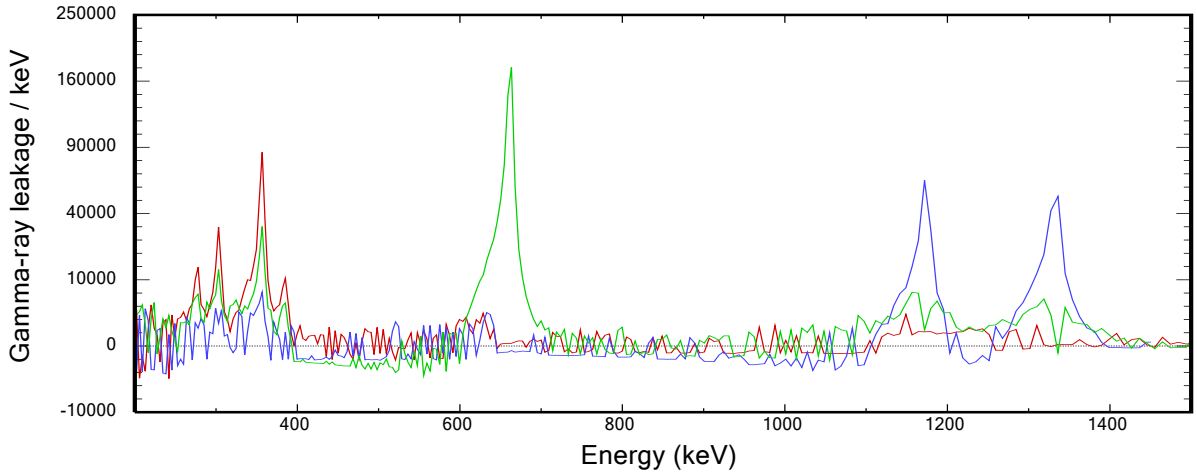

Figure 12. Angular source terms for calibration sources displaced 5 cm from center.

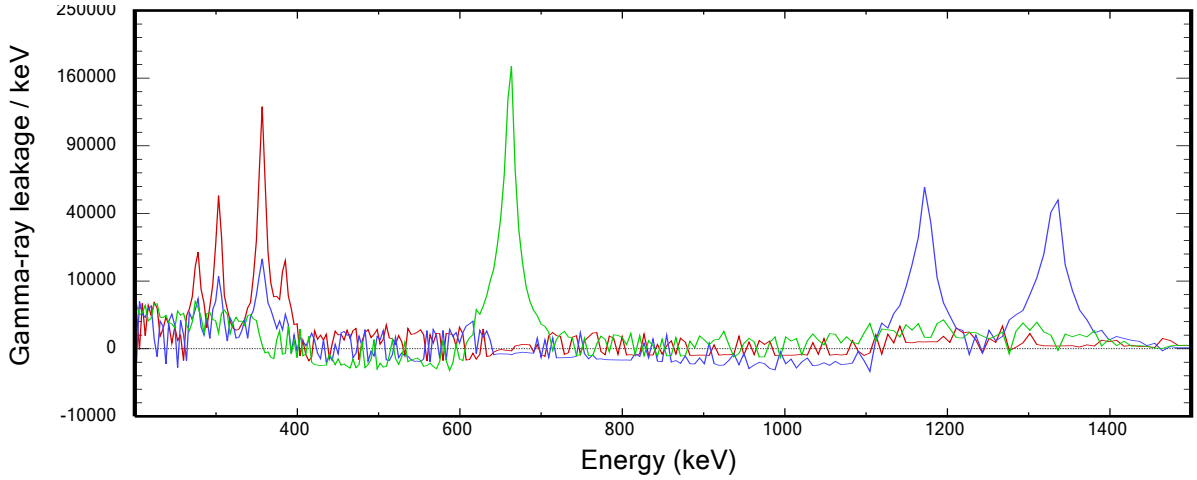

Figure 13. Angular source terms for calibration source displaced 10 cm from center.

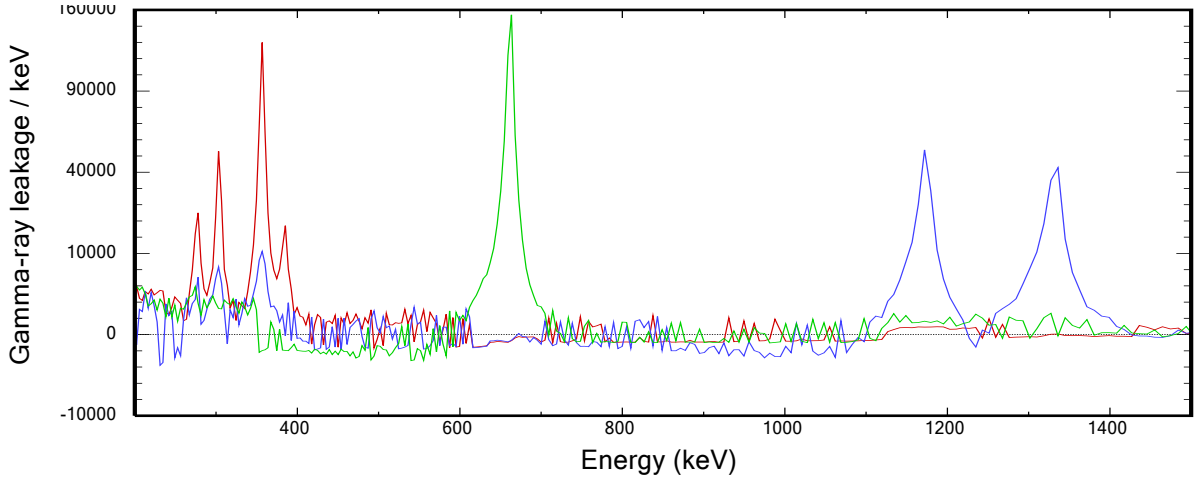

Figure 14. Angular source terms for calibration source displaced 15 cm from center.

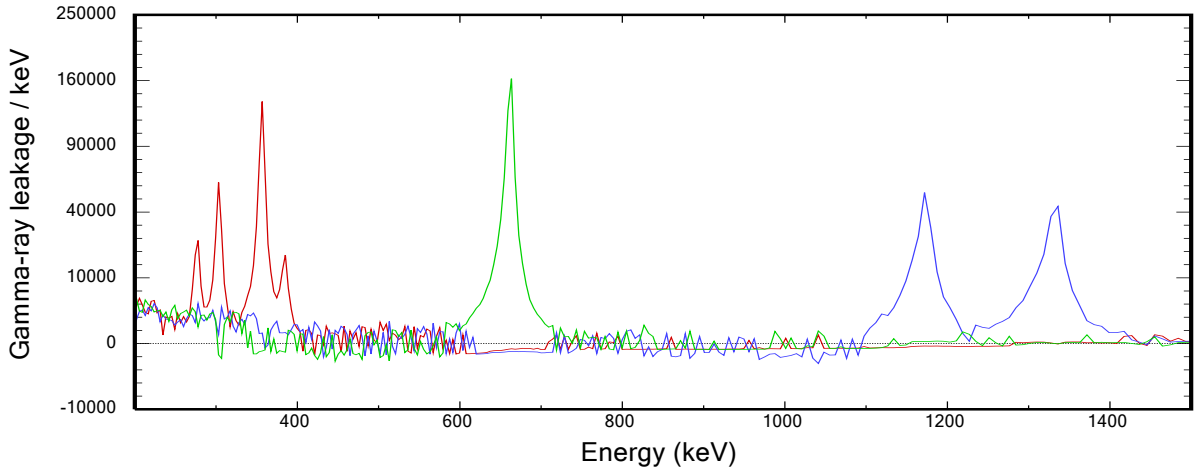

Figure 15. Angular source terms for calibration source displaced 20 cm from center.

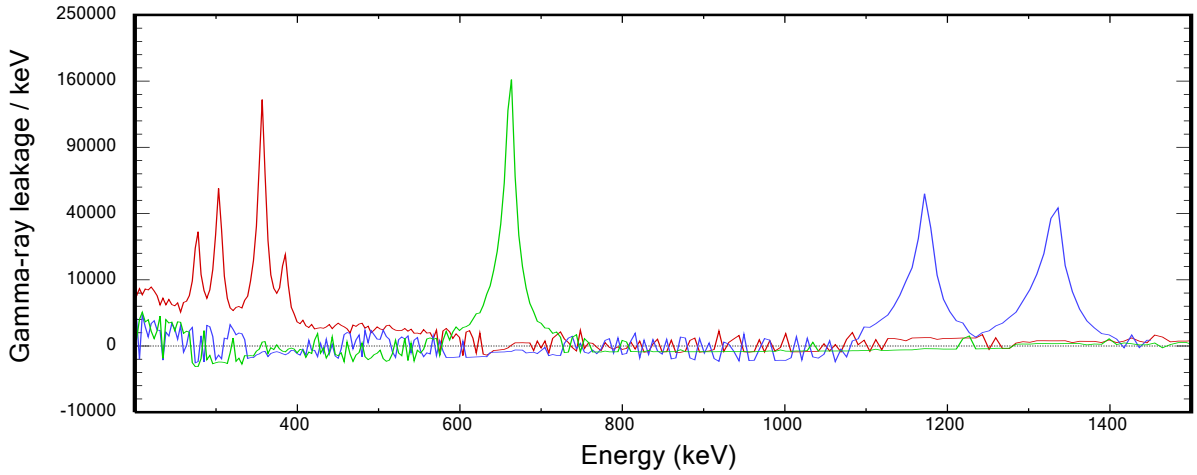

Figure 16. Angular source terms for calibration source displaced 30 cm from center.

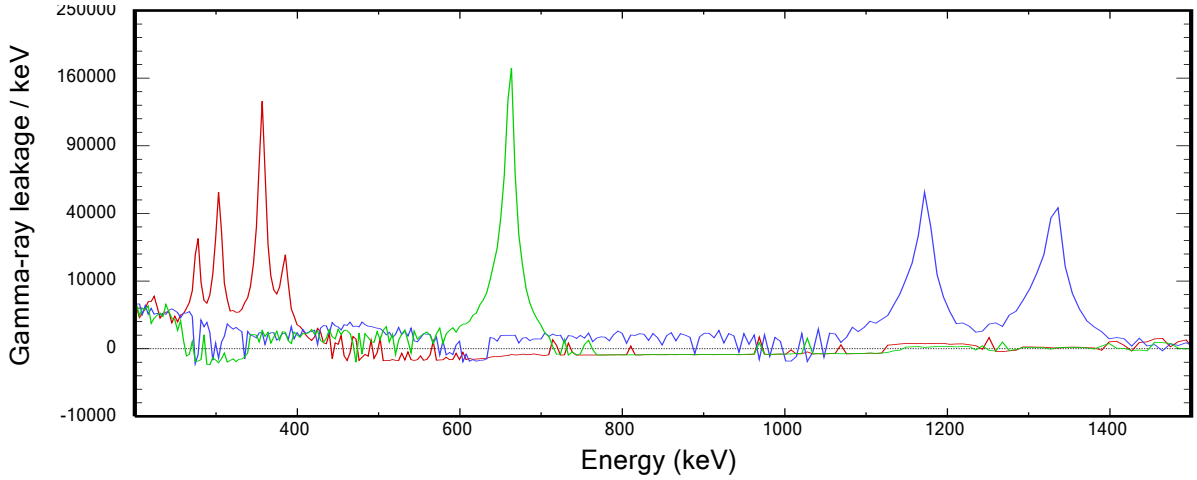

Figure 17. Angular source terms for calibration source displaced 50 cm from center.

6.2.2 Accuracy of the Computed Source Terms

Measured spectra are normally compared with calculations by applying a DRF to represent the way that a detector would respond to a specified radiation source. This is the preferred approach because uncertainties in the measured spectra are relatively easy to compute whereas uncertainties in unfolded spectra are more difficult to estimate. However, this protocol is not suitable for CCs because all angular regions contribute to the assessment, and a single spectrum cannot represent both the energy profiles and the spatial distribution of the profiles. Therefore, the GADRAS application was modified to suppress application of the normal DRF when CC source terms are viewed or analyzed. The only processing applied when spectra are computed is the application of spectral broadening associated with the normal peak shapes. Figures 18-20 compare the CC source terms at 10 cm displacements with computed spectra. These plots retain

the same color coding that is used elsewhere in this section of the report. The reduced chi-square (χ_r^2) values are displayed in these plots because they provide a metric for the quality of fit. Although the value of χ_r^2 should be unity if a perfect fit is obtained, estimation of the variance array is very difficult for processed spectra. Adjustments for the estimated uncertainties were made to address biases imposed by application of constraints to the linear regression procedure and double counting of input data because the background included regions that were also represented in the 10°-wide angular groups. Since these estimates are not rigorously accurate, χ_r^2 should be viewed as a qualitative metric as opposed to an absolute measure of the accuracy of the CC source terms.

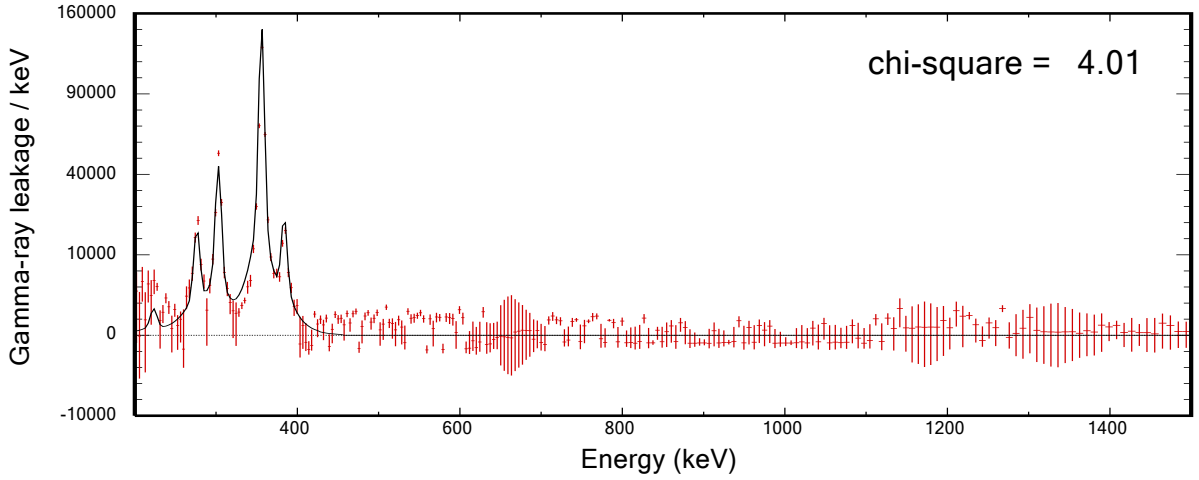

Figure 18. The CC source term (represented with ± sigma error bars) for the upper-left quadrant is compared with the computed spectrum (black) for the ^{133}Ba source. The sources were displaced by 10 cm from the center of the array.

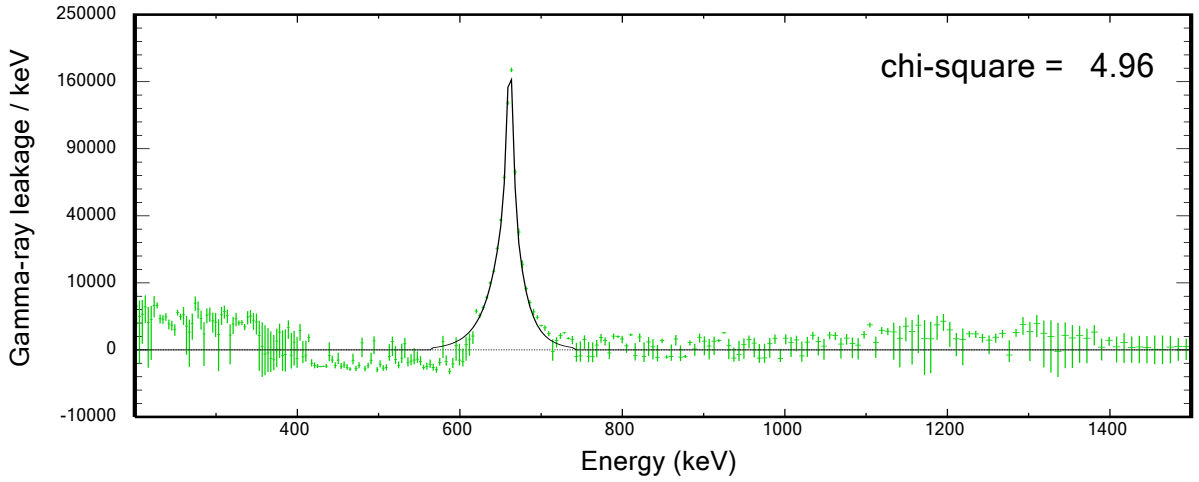

Figure 19. The CC source term (represented with ±1 sigma error bars) for the lower-right quadrant is compared with the computed spectrum (black)

for the ^{137}Cs source. The sources were displaced by 10 cm from the center of the array.

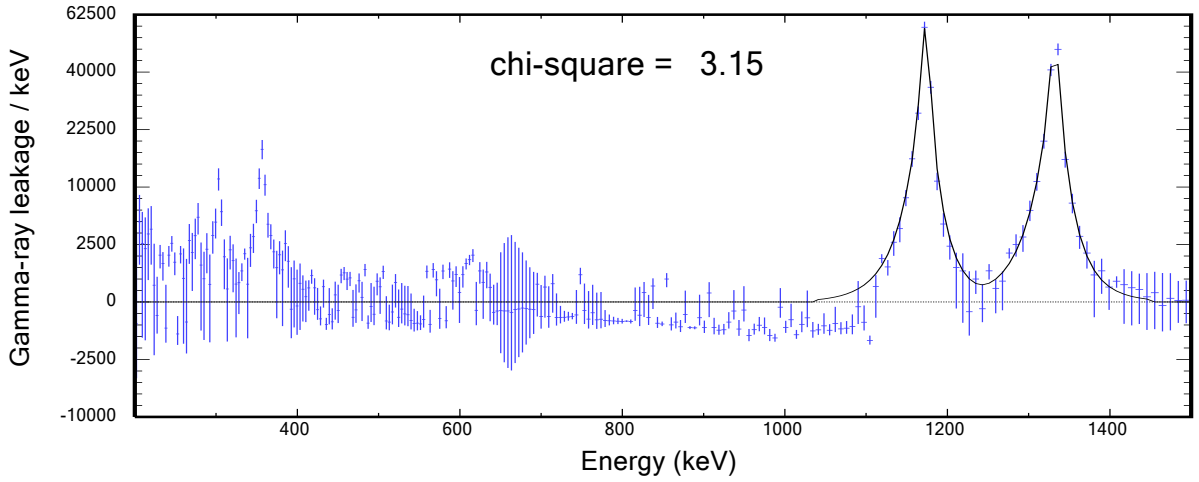

Figure 20. The CC source term (represented with ±1 sigma error bars) for the lower-left quadrant is compared with the computed spectrum (black) for the ^{60}Co source. The sources were displaced by 10 cm from the center of the array.

In order to compute the correct source leakages, distances used in the calculations were adjusted to account for slant angles. After applying this adjustment, source terms should represent the same leakages regardless of displacement relative to the center of the array if the calculations are correct. Accordingly, the two metrics that can be applied to evaluate the accuracy of the results are χ_r^2 and ratios of the computed gamma-ray relative to the actual emission rates of the calibration sources. Table 3 tabulates these metrics for all of the calibration source measurements. In order to focus on energy regions where gamma rays are emitted, the ratios of the CC source terms to the actual emission rates of the calibration sources are tallied in the ranges 250-400 keV, 600-700 keV, and 1100-1400 keV for the ^{133}Ba, ^{137}Cs, and ^{60}Co sources, respectively. The uncertainties in CC source terms are quite large at displacements of 1 cm and 2 cm, so the accuracy of the assessment is poor (particularly for ^{133}Ba) despite the low values of χ_r^2. The results for the ±50-cm displacements are highlighted in pink because the χ_r^2 values are quite large despite the fact that emission intensities are reasonably accurate. The discrepancy results from computation of excess continuum below the peaks (see Figure 17). This error is attributed to inaccuracy of the response function, which was characterized for sources normal to the detector axis, whereas sources were located 35 ° away from the axis in this case. It is certainly possible to characterize the response as a function of angle, but doing so adds a degree of complexity that may not be necessary depending on how the sensor is used.

Table 3. Calibration Sources Used During the ORNL Measurements

Displacement in X and Y directions	χ_r^2 / Ratio of CC Source to Known Gamma Leakage		
	^{133}Ba Quadrant	^{137}Cs Quadrant	^{60}Co Quadrant
1	0.25 / 0.42	0.27 / 0.95	0.37 / 0.80
2	0.23 / 0.53	0.56 / 1.2	0.64 / 0.96
5	2.7 / 0.64	4.91 / 1.2	2.63 / 0.94
10	4.0 / 0.90	5.0 / 1.1	3.15 / 0.98
15	0.44 / 0.91	0.40/ 0.92	0.48 / 0.91
20	0.58 / 1.0	0.49 / 1.1	0.59 / 0.96
30	2.2 / 1.1	0.93 / 0.97	1.22 / 0.97
50	46 / 0.77	34 / 1.0	52 / 1.2

6.3 ^{137}Cs Inside Polyethylene Sphere

A 7840-second measurement of the ^{137}Cs source inside a 3-inch-thick polyethylene (PE) ball was performed at ORNL. The inside and outside radii of the PE ball were 11.5 cm and 19.1 cm, respectively. The energy-resolved intensity profile presented in Figure 21 suggests that the object is larger than a point source, but the extent of the object cannot be determined accurately.

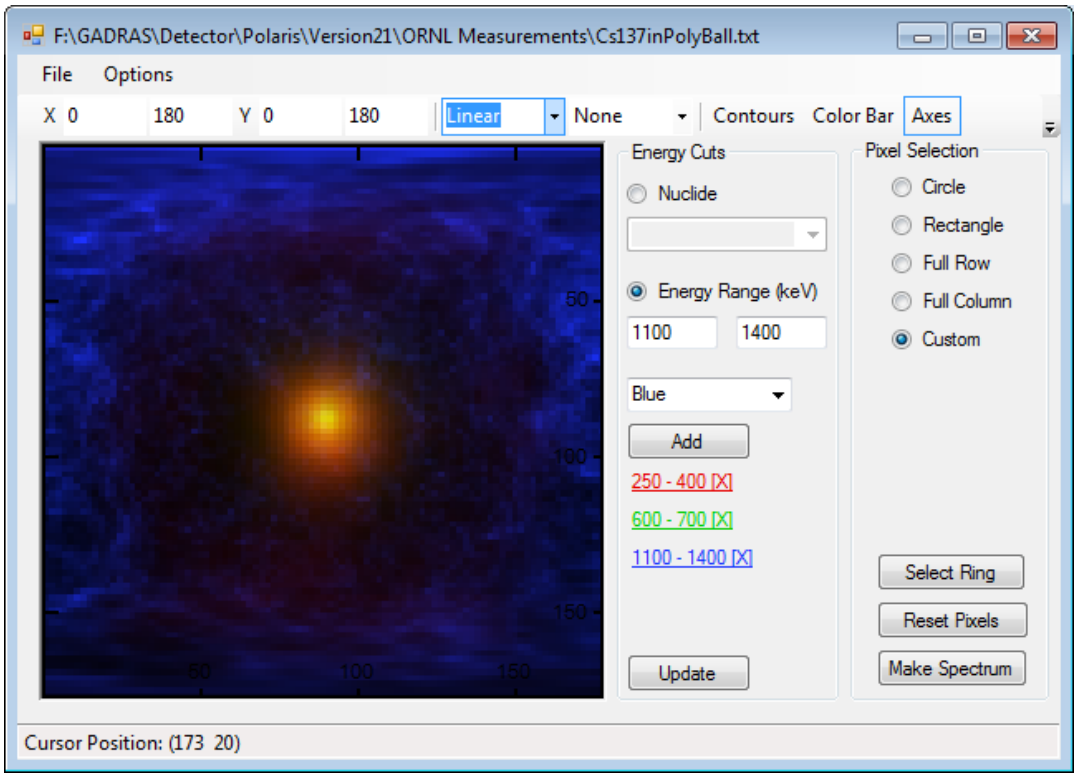

Figure 21. Energy-resolved intensity profile for the ^{137}Cs source inside the 3″ PE ball.

At a distance of 100 cm, the outside radius of the PE corresponds to an angle of 10.8° relative to the center of the sphere, which is about the same as the limiting resolution, at least for low-energy gamma rays. In order to evaluate the possibility that scattered radiation can be distinguished from un-collided gamma rays, a DUST input file was created that represented background plus two concentric circles, with angular ranges of 0:10° and 10:20°. Figure 22 shows that the CC source term for the sum of the two spatial groups is in good agreement with the gamma-ray leakage computed for a model of the source. Un-scattered gamma rays are emitted from the center of the object (i.e., within the 0:10° group), and the 10:20° group exhibits a continuum that is consistent with scattered radiation. A similar analysis was performed using data for the bare ^{137}Cs source (see Figure 23). In this case, the continuum is virtually absent from both angular groups, which confirms that the assessed continuum for the shielded source is representative of scattered radiation. Although these results demonstrate that the presence of scattering materials can be inferred by the directional spectra, the angular resolution is not sufficient to extract more detailed information such as the diameter of the void within the PE sphere.

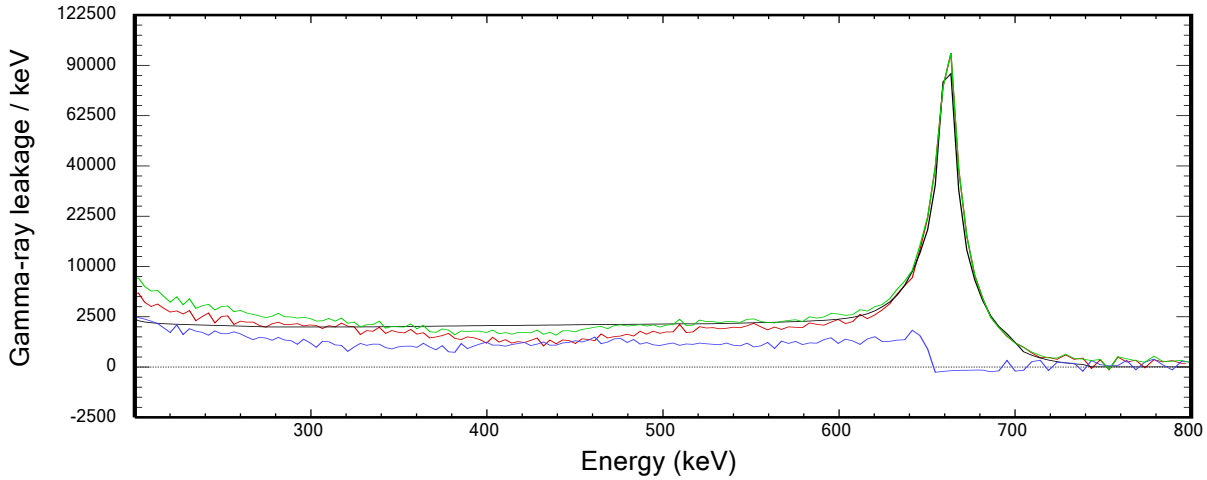

Figure 22. The computed leakage spectrum based on a 1-D model of the ^{137}Cs source inside the 3″-thick PE sphere (black) is compared with the CC source terms for the 0:10° angular group (red) the 10:20° group (blue). The green curve shows the sum of the CC source terms for the 0:10° and 10:20° angular groups.

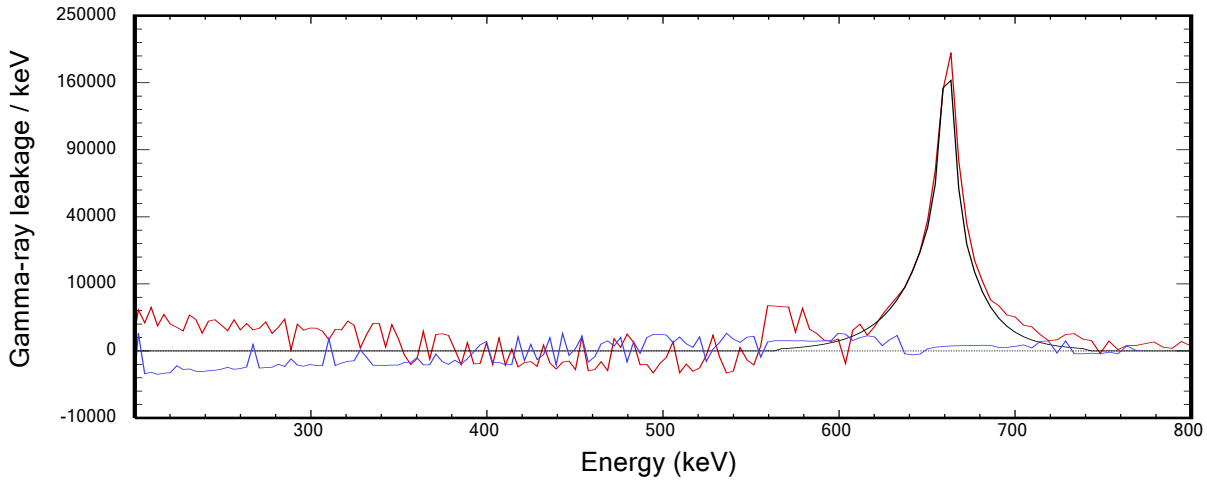

Figure 23. The emission profile of the ^{137}Cs source (black) is compared with the CC source terms for the 0:10° angular group (red) and 10:20-degree group (blue).

6.4 Depleted Uranium Castings

Several measurements were collected for depleted uranium (DU) castings in various configurations. One of the castings was an 18-kg hollow cylinder with an inside radius of 4.4 cm, an outside radius of 6.4 cm, and a length of 15.2 cm. The DU is enclosed within a 2-mm-thick steel shell. The other casting has about the same diameter but about half the mass and half the

length. The DUST algorithm was able to deduce spectral profiles for 10-minutes measurements of these objects, but the statistical confidence is low and it is difficult to resolve features in plotted spectrum. Since gamma ray emission profiles were essentially the same for all of the DU measurements, only one example is presented in this section. In this configuration, shown in Figure 24, the castings are separated by a 25-cm gap and the axes are aligned. The energy-resolved profile displayed in Figure 25 varies from black to white across the visual field, which is consistent with a uniform gamma-ray emission profile. Figure 26 displays a gross intensity profile, which also shows that the object is elongated in the horizontal direction and that the intensities differ on the two ends. The preference for which intensity profile conveys the most information is subjective.

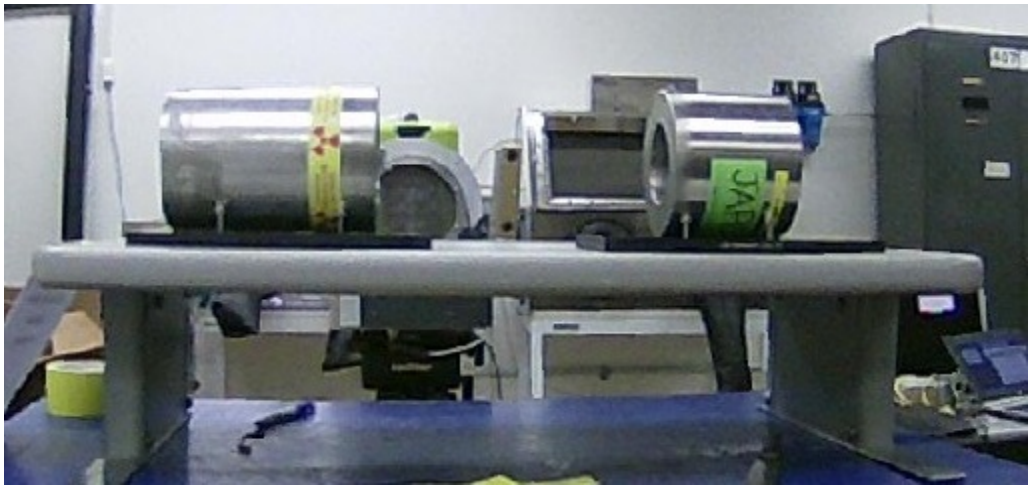

Figure 24. Photograph of the 18 kg and 9 kg DU castings supported by a table. The GeGl detector is on the far side and to the right of the larger DU casting.

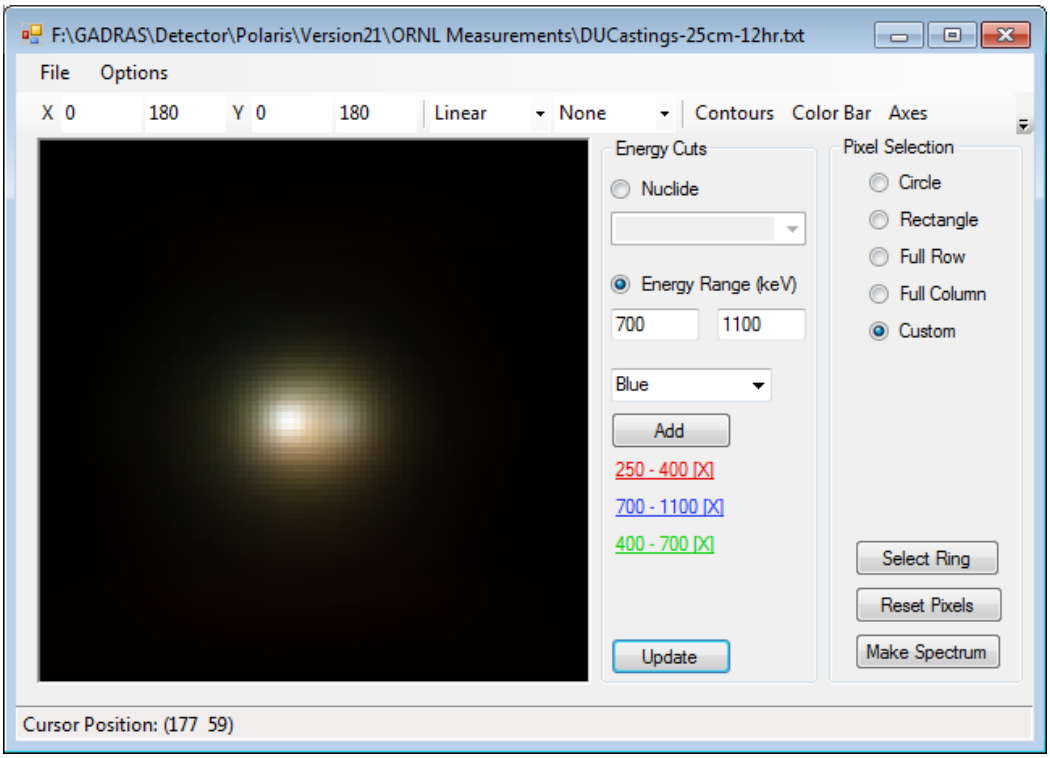

Figure 25. Energy resolved gamma-ray profile for the two DU castings.

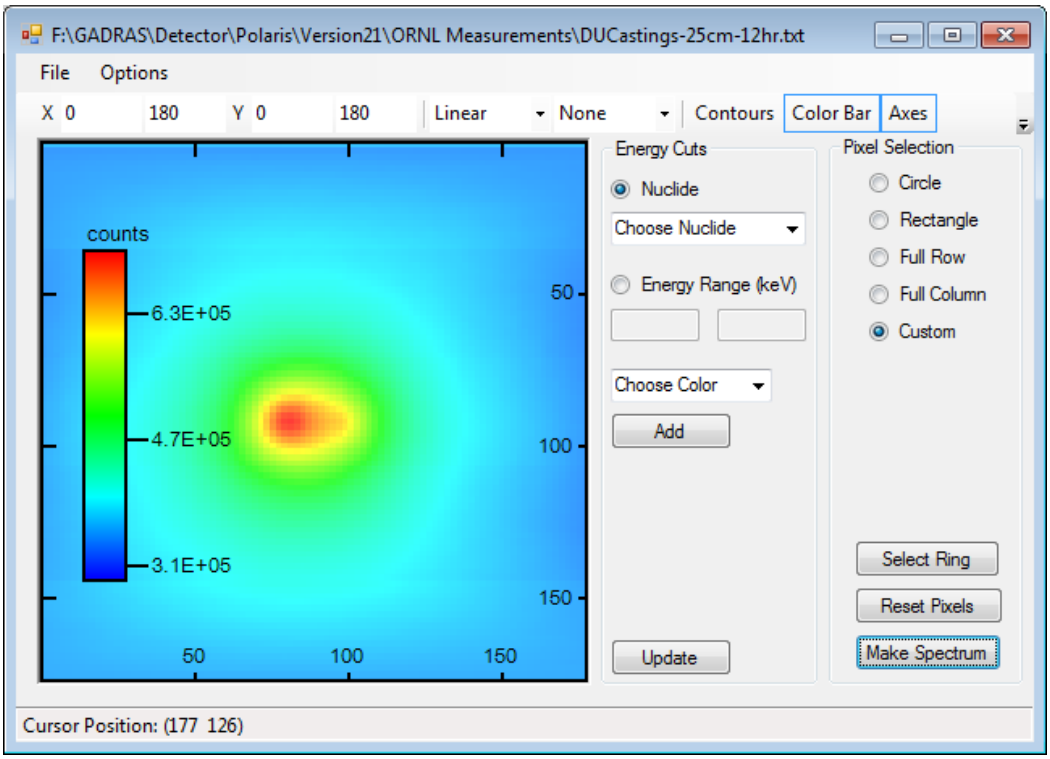

Figure 26. Gross gamma-ray intensity profile for the two DU castings.

Computation of the source profiles for the DU objects tests the ability to estimate the continuum produced by Bremsstrahlung radiation, which represents about half of the total leakage. The directional back-projection spectra that were used as input for the DUST algorithm utilized a background group plus 10°-wide angular groups with centers separated by 21°. Leakage profiles computed on the left and right sides of the assembly are shown in Figure 26. The ratio of the integrated CC source terms for the left versus right sides of the scene is 1.5, whereas the larger DU casting emits about twice as many gamma rays as the smaller casting. The ratio of the computed CC source intensities varied with the asserted positions of the objects, which cannot be determined with an accuracy better than a few degrees based in the profiles shown in Figures 25 and 26.

The ability to link 3-D source models with directional sensors has not been completely integrated into GADRAS, so the CC source terms are compared with a 1-D model of the larger of the two castings. The computed leakage profile is in good agreement with shapes of the two CC source terms above 400 keV, and the intensities are reasonably consistent given the aforementioned uncertainties associated with the positions of the castings and the 1-D approximation for the source leakage.

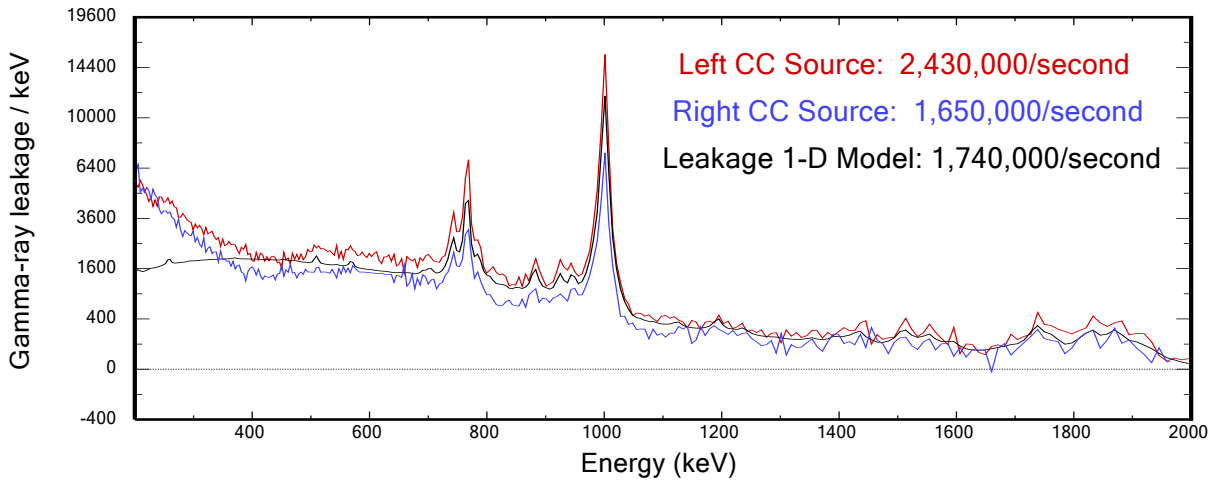

Figure 27. CC source terms that are computed for the two DU castings separated by 25 cm (red and blue curves for the left and right sides, respectively) are compared with the gamma-ray leakage for the larger of the two castings (black).

Background source terms have not been displayed previously because they clutter the plots and generally do not add much useful information. However, the CC source term for the background group is instructive in this case. Figure 27 compares the CC source term for the background group that was computed while the detector was exposed to the DU castings with the background spectrum that was computed when no additional sources were present. The source terms exhibit prominent peaks at 1460 keV and 2614 keV, which are associated with emission from ^{40}K and ^{232}Th, respectively, and small peaks at 583 keV and 609 keV from ^{232}Th and ^{226}Ra. As in all other DUST calculations, the estimated background radiation was stripped from the localized

source terms, so these peaks only appear in the background group unless localized sources also emit gamma rays at these energies. An observation that is relevant with respect to understanding differences between source terms for the DU castings and the computed leakage derived from the model of the casting is that scattered radiation from the DU castings increases the background source term at low energy. The current DUST algorithm treats scattered radiation as an isotropic source, which is a gross approximation. Therefore, we suspect that the increased leakage below 400-keV for the CC source terms shown in Figure 26 relative to the computed leakage for a model of the DU casting is associated with 3-D effects that are not modeled correctly.

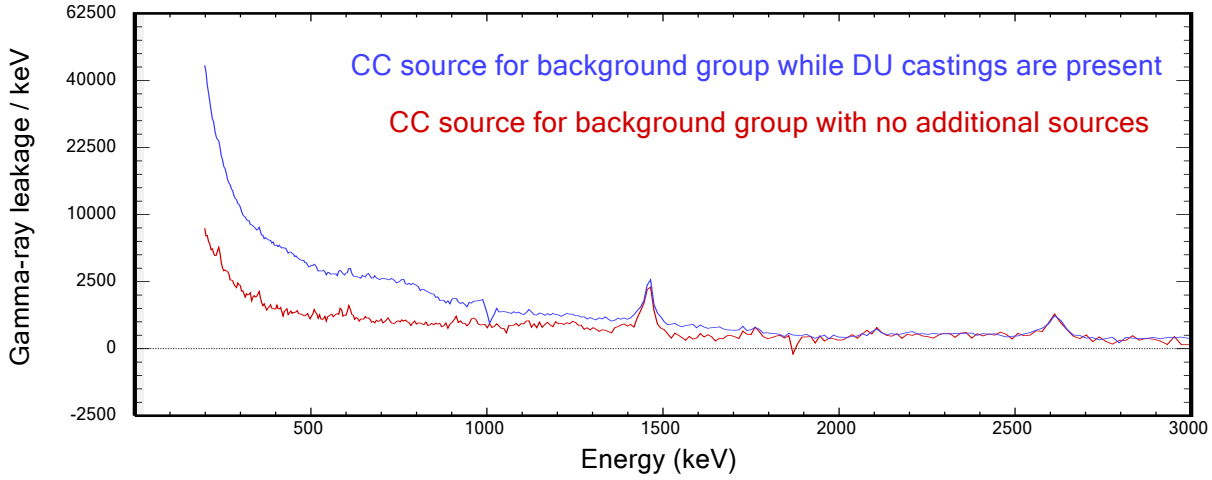

Figure 28. The background CC source term that is computed while the two DU castings were present (blue) exhibits a substantially greater low-energy continuum than the source term that is computed while no sources were present.

This page in intentionally blank.

7 CONCLUSIONS

This document presents an evaluation of our approach for processing data collected by the Polaris system while operated in CC mode. The process is summarized below:

- Select local spatial regions that exhibit characteristics of interest, which can be accomplished either by observing locations of objects in an optical image or by inspecting a gamma-ray intensity profile. Color coding different energy regions enhances the information content relative to gross intensity profiles.
- Back-projection spectra are created for the background group (i.e., all imageable events) plus back-projection spectra for each of the spatial regions of interest. For the calibration sources, the best results were obtained using 10°-wide angular groups that were centered on the actual source locations. The angular groups can overlap if the sources are separated by less than 10°. Alternatively, a series of concentric circles is more suitable for a generally spherical object, such as the ^{137}Cs source inside the polyethylene shell.
- The DUST algorithm was used to compute the CC source terms. The algorithm was able to differentiate gamma-rays from ^{137}Cs and ^{60}Co when the sources were separated by less than 2°, but a separation of greater than 10° was required to isolate the ^{133}Ba emission from gamma rays emitted by other sources. The spatially resolved source terms were consistent with emission profiles from the calibration sources and from models of spatially-extended sources. The accuracy could be improved by addressing the dependence of the DRF on the angle of incidence with the detector and completing the linkage between GADRAS and the DUST algorithm with respect to 3-D sources. Nevertheless, the current accuracy is sufficient to enable isotope identification and activity estimates for bare sources, and radiation continua are replicated with sufficient accuracy to enable crude shielding estimates.

The inability to observe low-energy gamma rays is an obvious deficiency associated with CCs, so our analysis algorithms will need to utilize CA spectra to completely utilize data that is available from sensors like Polaris. An obvious way to accomplish this objective is to combine source terms that are computed by CC and CA methods. Although the spectral stripping approach utilized in the DUST method could be applied, spectra that are determined by the CA approach exhibit much less covariance than data derived from CCs. A sophisticated flux estimation tool that already exists in GADRAS could be applied to derive source terms from CA spectra.

As described above, additional work is needed to complete the development of user-based analysis procedures for imaging spectrometers. The current methods are cumbersome, and need to be made more operationally transparent to be useful to less experienced analysts.

We plan to investigate implementation of an automated approach that could produce isotope specific activity or dose profiles. Doing so will require substantially more processing relative to what was described in this document because back-projection spectra must be produced for each spatial element, and response functions must account for covariances among the spatial elements. This automated and unconstrained processing approach could fail either because the statistical

uncertainties are too large for numerous small spatial groups or because the computational time is excessive. However, regardless of the success of an automated approach, analysts will want to retain manual control of data processing, so the essence of the analysis approach described in this document will likely be retained.

This document focused on the development of methods for using CC data to synthesize spectra that are compatible with analysis methods applicable to gross gamma-ray spectrometers. Future work will investigate the relative merits of directional spectra versus gross gamma-ray spectra produced by sensors such as Polaris or by other types of instruments.

8 REFERENCES

[1] "The DirectSoftware Project," is sponsored by DOE/NNSA/NA-221 as project number SL15-V-DirectdSoftware-PD2Jc.

[2] D. J. Mitchell, H. M. Sanger and K. W. Marlow, "Gamma-Ray Response Functions for Scintillation and Semiconductor Detectors, Nucl. Inst. and Meth. A276," 1989.

[3] D. J. Mitchell and J. Mattingly, "Rapid Computation of Gamma-ray Spectra for One-Dimensional Source Models," American Nuclear Society 2008 Annual Meeting, June 2008.

[4] D. J. Mitchell, "Variance Estimation for Radiation Analysis and Multi-Sensor Fusion," 2010 IEEE Nuclear Science Symposium Conference Recorded, N43-2 pp 1220-128, 2010.

[5] D. Xu and Z. He, "Gamma-ray energy-imaging integrated spectral deconvolution," Nuclear Instruments and Methods in Physics Research Section A: Accelerators, Spectrometers, Detectors and Associated Equipment 574, no. 1 (2007): 98-109.

DISTRIBUTION

1 DOE/NNSA/NA-221
Attn: David Lagraff (electronic copy)
David.Lagraffe@nnsa.doe.gov

2 DOE/NNSA/NA-221
Attn: Kevin Jackman (electronic copy)
Kevin.Jackman@nnsa.doe.gov

3 Defense Threat Reduction Agency
Attn: Marc Black (electronic copy)
Marc.Black.ctr@mail.mil

4. Defense Threat Reduction Agency
Attn: Daniel Mannis (electronic copy)
Daniel.N.Mannis.mil@mail.mil

5. H3D, Inc.
Attn: Dr. Willy Kaye (electronic copy)
Founder and CEO
willy@h3dgamma.com

6. H3D, Inc.
Attn: Dr. Jason Jaworski (electronic copy)
Engineer
jason@h3dgamma.com

7. University of Michigan
Attn: Zhong He, Professor, (electronic copy)
Nuclear Engineering and Radiological Sciences
hezhong@umich.edu

1	MS0155	Clint Hall	6634 (electronic copy)
1	MS0782	Dean Mitchell	6634 (electronic copy)
1	MS0782	Steven Horne	6634 (electronic copy)
1	MS0782	Greg Thoreson	6634 (electronic copy)
1	MS0782	Lee Harding	6634 (electronic copy)
1	MS0899	Technical Library	9536 (electronic copy)

This page in intentionally blank.


Sandia National Laboratories